Online Appendices to

On Figures of Merit for Randomly-Shifted Lattice Rules

Pierre L'Ecuyer and David Munger

In these appendices, we present the estimations of the ANOVA variances and the experimental results that support our observations in Sections 9 to 11 in the published paper, where the analysis is already complete.

13 An Indicator Function

We present here the results for the indicator function described in Section 9 of the main paper. The estimated ANOVA variances for the most important projections with $s = 6$ are shown in Figure 9. For lattices constructed with $\mathcal{P}_{\gamma,2}$ with projection-dependent weights, examples of the observed and fitted variances are shown in Figure 10 and the empirical convergence rates are displayed in Table 3.

In the last paragraph of Section 9 in the main paper, we report on experiments with a simpler case with $s = 2$ where $Y_1 \sim U[0, m)$ for some $m \in [0, 1)$ and $Y_2 \sim U[0, 1)$. This corresponds to an integrand whose discontinuity is a straight line of slope $-m$, linking the points $(0, x)$ and $(1, x + m)$:

$$f(\mathbf{u}) = f(u_1, u_2) = \mathbb{I}[u_2 > x - mu_1], \tag{19}$$

where m and x are constants such that $0 \le x \le 1$ and $x - 1 \le m \le x$. This is illustrated in Figure 11 for $x = 0.8$ and $m = 0.375$. The shaded area is the region where the indicator equals 1.

The Fourier coefficients of this integrand are

Pierre L'Ecuyer and David Munger
Département d'Informatique et de Recherche Opérationnelle, Université de Montréal, C.P. 6128, Succ. Centre-Ville, Montréal, H3C 3J7, Canada, lecuyer@iro.umontreal.ca, mungerd@gmail.com

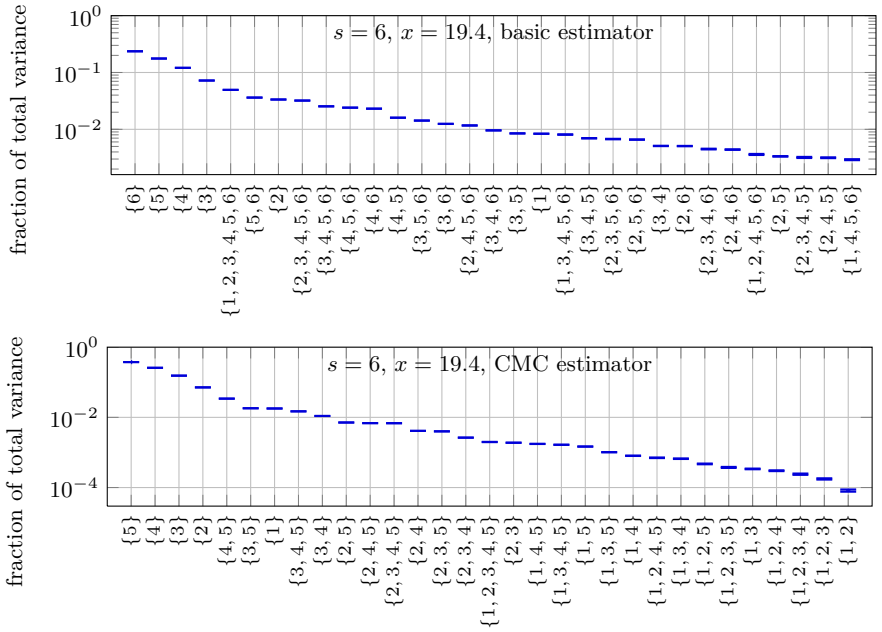

Fig. 9 Fractional ANOVA variances per projection for the indicator of a sum of independent exponentially distributed variables $s = 6$, $x = 19.4$ and $\lambda_j = j^{-1}$, for the basic estimator (top) and the CMC estimator (bottom). For the basic estimator, only the 31 more important projections out of $2^6 - 1 = 63$ total projections are displayed. The projections are listed on the horizontal axis, and their fraction of total variance is plotted along the vertical axis. The limits of each vertical bar correspond to a normal confidence interval at 95 % on the variance estimate, the standard deviation of which was estimated across independent random draws. Note the different scales on the vertical axes.

$$\hat{f}(h_1, h_2) = \frac{\mathrm{e}^{-2\pi \mathrm{i} h_2 x}\left[\mathrm{e}^{-2\pi \mathrm{i}(h_1 + h_2 m)} - 1\right]}{4\pi^2 h_2 (h_1 + h_2 m)},$$

for $h_1 + h_2 m \neq 0$, and

$$\hat{f}(h_1, h_2) = \frac{\mathrm{e}^{-2\pi \mathrm{i} h_2 x}}{2\pi \mathrm{i} h_2}$$

for $h_1 + h_2 m = 0$. Note that if $x = 1$ and $m = -1$, the discontinuity is a diagonal and the only non-vanishing Fourier coefficients are those for which $h_1 + h_2 m = 0$. Let θ and φ denote the angles from the positive x_1 axis to $\mathbf{h}$ and the perpendicular to the discontinuity, respectively, such that $\mathbf{h}/\|\mathbf{h}\| = (\cos\theta, \sin\theta)$ and $m = -\cot\varphi$. For $\theta \neq \varphi$, we have

$$\left|\hat{f}(h_1, h_2)\right|^2 = \frac{\sin^2\varphi\,[1 - \cos(2\pi\|\mathbf{h}\|\eta)]}{8\pi^4\|\mathbf{h}\|^4 \sin^2\theta \sin^2(\theta - \varphi)}, \tag{20}$$

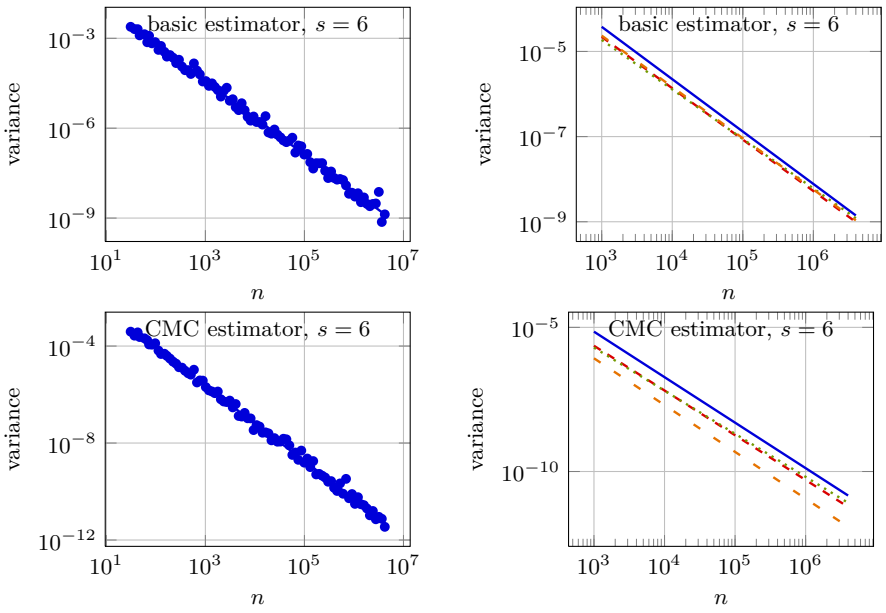

Fig. 10 Estimated variance (left) and fitted variance (right) of the basic (top) and CMC (bottom) RQMC estimators for the indicator of the sum of exponential variables, for $s = 6$, with $\lambda_j = 1$ and $x = 5.7$ (——). On the right, we also have the plots for $\lambda_j = j^{-1}$ and $x = 19.4$ (- - -), for $\lambda_j = j^{-1}$ and $x = 33.5$ (·····), and for $\lambda_j = j^{-2}$ and $x = 81.5$ (- -). The lattices were constructed with the $\mathcal{P}_{\gamma,2}$ criterion using projection-dependent weights, and the baker's transformation was not applied.

where $\eta = \csc\varphi \sin(\theta - \varphi)$, and $\csc\varphi$ represents the length of the segment of discontinuity. For $\theta = \varphi$, we have

$$\left|\hat{f}(h_1, h_2)\right|^2 = \frac{1}{4\pi^2 \|\mathbf{h}\|^2 \sin^2 \varphi},$$

which is also the limit of (20) when $\theta \to \varphi$ for fixed $\|\mathbf{h}\|$ and φ. It is easy to check that, for fixed $\|\mathbf{h}\|$ and φ, $|\hat{f}(h_1, h_2)|^2$ has a local maximum in $\theta = \varphi$.

In Figure 11, we show three examples of lattices with $n = 97$ that perform well (on the left panel) in terms of the RQMC variance for the indicator function (19) and three examples of lattices that perform very poorly (on the right panel). The RQMC variances of those on the right are (approximately) from 20 to 200 times larger than for those on the left. For $n = 97$, $\mathcal{P}_2$ reaches its minimum value of 1.53×10^{-2} at $a_2 = 35$, 36, 61, and 62. The values $a_2 = 35$ and $a_2 = 36$ correspond to the two lattices whose points look the most evenly distributed in the figures, one on the left and one on the right. Interestingly, the RQMC variance of the second is more than 20 times that of the first! This happens because for the second lattice, the points are in lines that are perfectly aligned with the discontinuity. Thus, when one line

s	λ_j	x	$\hat{\mu}_{n,\text{rqmc}}$	$\hat{\nu}$		
				basic (no baker)	CMC (no baker)	CMC (with baker)
2	1	1.7	0.5	1.522 ± 0.006	1.998 ± 0.001	3.980 ± 0.010
	j^{-1}	2.5	0.5	1.549 ± 0.006	1.998 ± 0.001	3.940 ± 0.010
	j^{-1}	6.0	0.1	1.517 ± 0.005	1.998 ± 0.001	4.000 ± 0.010
	j^{-2}	10.4	0.5	1.501 ± 0.004	1.995 ± 0.002	3.710 ± 0.010
3	1	2.7	0.5	1.363 ± 0.007	1.931 ± 0.002	2.390 ± 0.010
	j^{-1}	5.2	0.5	1.341 ± 0.008	1.929 ± 0.002	2.380 ± 0.010
	j^{-1}	11.0	0.1	1.336 ± 0.005	1.955 ± 0.002	2.190 ± 0.010
	j^{-2}	11.6	0.5	1.294 ± 0.008	1.907 ± 0.002	2.233 ± 0.009
4	1	3.7	0.5	1.288 ± 0.007	1.823 ± 0.004	1.919 ± 0.009
	j^{-1}	9.0	0.5	1.298 ± 0.007	1.814 ± 0.004	1.831 ± 0.008
	j^{-1}	17.3	0.1	1.273 ± 0.005	1.825 ± 0.003	1.702 ± 0.005
	j^{-2}	26.0	0.5	1.250 ± 0.008	1.860 ± 0.003	1.743 ± 0.006
5	1	4.7	0.5	1.239 ± 0.006	1.629 ± 0.008	1.643 ± 0.006
	j^{-1}	13.8	0.5	1.238 ± 0.006	1.638 ± 0.007	1.615 ± 0.006
	j^{-1}	25.0	0.1	1.212 ± 0.006	1.631 ± 0.005	1.524 ± 0.004
	j^{-2}	48.9	0.5	1.234 ± 0.007	1.671 ± 0.006	1.647 ± 0.005
6	1	5.7	0.5	1.226 ± 0.005	1.578 ± 0.006	1.454 ± 0.005
	j^{-1}	19.4	0.5	1.230 ± 0.005	1.552 ± 0.005	1.478 ± 0.005
	j^{-1}	33.5	0.1	1.207 ± 0.003	1.495 ± 0.005	1.418 ± 0.005
	j^{-2}	81.5	0.5	1.205 ± 0.006	1.623 ± 0.007	1.548 ± 0.005

Table 3 Estimated convergence rates $\hat{\nu}$ for the indicator of a sum of random variables, with all significant figures, with lattices constructed with the $\mathcal{P}_{\gamma,\alpha}$ criterion with $\alpha = 1$ without baker and $\alpha = 2$ with baker. The reported precision on $\hat{\nu}$ corresponds to the half-width of a 95 % confidence interval. The actual values for $\hat{\mu}_{n,\text{rqmc}}$ are within 1 % of the displayed value for n large enough.

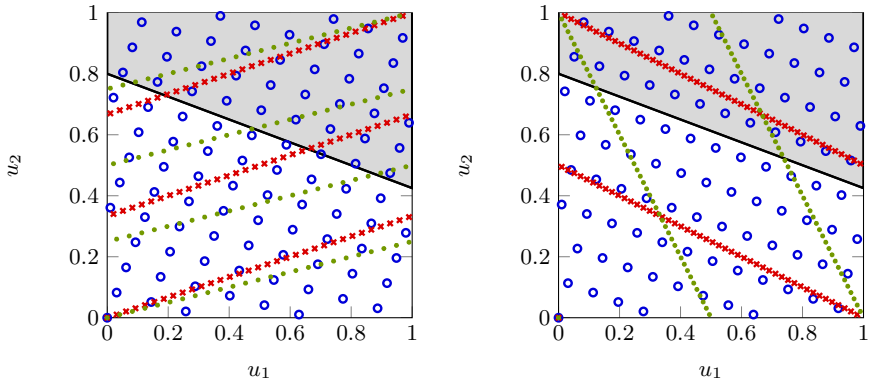

Fig. 11 Integration of an indicator function of the form (19), using RQMC with six different lattices with $n = 97$. The indicator is 1 in the shaded area. The discontinuity has slope $m = -0.375$ and passes through points $(0, 0.8)$ and $(1, 0.425)$. The three (good) lattices on the left have $a_2 = 35$ (o), $a_2 = 65$ (×), and $a_2 = 73$ (·). Their RQMC variances are 3.78×10^{-5}, 6.71×10^{-5} and 8.92×10^{-5}, respectively. The three (bad) lattices on the right have $a_2 = 36$ (o), $a_2 = 48$ (×), and $a_2 = 95$ (·). Their RQMC variances are 1.33×10^{-3}, 1.14×10^{-2} and 1.73×10^{-3}, respectively.

of points jumps across the discontinuity due to a small change in the shift, this causes a large change in the estimate, whence the larger variance. This alignment also corresponds to a short dual vector $\mathbf{h} \in L_2^*$ perpendicular to the discontinuity. One lattice on the left (with $a_2 = 65$) has all its points regrouped in only three lines, so usual figures of merit are typically bad for this lattice, yet it performs quite well for this particular integrand. This shows that good lattices here do not necessarily have evenly distributed points, and conversely; the variance depends more on the alignment between the lattice structure and the discontinuity.

14 Example: a Stochastic Activity Network

In this section, we show the results for the stochastic activity network described in Section 10. The ANOVA variances per projection are shown in Figure 12 for $x = 60$, and per projection order in Figure 13 for all selected values of x. Among the 10 projections contributing the most variance for the basic estimator, excluding the one-dimensional projections, four belong to paths linking the source to the sink and six (including the most important one, $\{10, 13\}$), do not. The situation is different for the CMC estimator: most of the variance belongs to projections taken from the path $\{1, 4, 8, 9, 13\}$, which is the single path going through edge 9. This suggests that the variability of the term $\mathbb{P}[V_9 \le x - P_9]$, dominates the variance of the CMC estimator (18). Thus, the V_j's that sum up to P_9 contribute most of the variance.

The results for the basic RQMC estimator without the baker's transformation are summarized in Table 4. In all cases, the criterion $\mathcal{P}_{\gamma,2}$ consistently has relatively high values of $\widehat{\mathrm{VRF}}(2^{20})$ and $\hat{\nu}$, with low values of $\hat{S}_\varepsilon$, but it does not always clear dominate, as we can see in Table 4 for $x = 85$.

For the CMC estimator, using $\mathcal{M}_{\gamma,2}$ or $\mathcal{M}'_{\gamma,2}$, in contrast to using the $\mathcal{P}_{\gamma,2\alpha}$ criteron, generally results in more noise in the observed RQMC variances, as illustrated in Figure 14. This discrepancy can be larger or smaller for different values of x, but appears independent of x.

We show some results for the estimation of $\mathbb{E}[T]$ with the $\mathcal{P}_{2\alpha}$ criterion in Table 5. Curiously, the product weights provide the smallest RQMC variances (largest $\widehat{\mathrm{VRF}}(2^{20})$ and $\hat{\nu}$). The projection-dependent weights are not far behind.

basic estimator, $x = 60$

criterion	weight type	$\widehat{\mathrm{VRF}}(2^{20})$	$\hat{\nu}$	$\hat{S}_\varepsilon$
$\mathcal{P}_{\gamma,2}$	product	21	1.201 ± 0.007	0.524
$\mathcal{P}_{\gamma,2}$	proj.-dep.	27	1.201 ± 0.003	0.196
$\mathcal{P}_{\gamma,2}$	order-dep.	18	1.182 ± 0.005	0.346
$\mathcal{M}_{\gamma,2}$	geometric	14	1.180 ± 0.010	0.782
$\mathcal{P}_{\gamma,2}$	geometric	17	1.168 ± 0.009	0.640
$\mathcal{M}'_{\gamma,2}$	order-dep.	16	1.167 ± 0.005	0.390
$\mathcal{M}'_{\gamma,2}$	geometric	17	1.165 ± 0.007	0.488
$\mathcal{M}_{\gamma,2}$	product	14	1.161 ± 0.008	0.611
$\mathcal{M}'_{\gamma,2}$	proj.-dep.	18	1.156 ± 0.005	0.359
$\mathcal{M}'_{\gamma,2}$	product	16	1.154 ± 0.005	0.379
$\mathcal{M}_{\gamma,2}$	proj.-dep.	14	1.146 ± 0.009	0.671
$\mathcal{M}_{\gamma,2}$	order-dep.	13	1.138 ± 0.008	0.565

basic estimator, $x = 85$

criterion	weight type	$\widehat{\mathrm{VRF}}(2^{20})$	$\hat{\nu}$	$\hat{S}_\varepsilon$
$\mathcal{P}_{\gamma,2}$	geometric	26	1.222 ± 0.006	0.334
$\mathcal{M}_{\gamma,2}$	geometric	21	1.220 ± 0.010	0.737
$\mathcal{P}_{\gamma,2}$	product	28	1.211 ± 0.007	0.486
$\mathcal{M}'_{\gamma,2}$	product	26	1.201 ± 0.006	0.459
$\mathcal{M}'_{\gamma,2}$	geometric	22	1.187 ± 0.008	0.566
$\mathcal{P}_{\gamma,2}$	proj.-dep.	28	1.184 ± 0.004	0.290
$\mathcal{M}'_{\gamma,2}$	proj.-dep.	25	1.181 ± 0.007	0.529
$\mathcal{M}_{\gamma,2}$	product	21	1.177 ± 0.007	0.511
$\mathcal{M}_{\gamma,2}$	order-dep.	21	1.175 ± 0.007	0.489
$\mathcal{M}'_{\gamma,2}$	order-dep.	22	1.166 ± 0.007	0.558
$\mathcal{P}_{\gamma,2}$	order-dep.	22	1.165 ± 0.006	0.463
$\mathcal{M}_{\gamma,2}$	proj.-dep.	18	1.136 ± 0.008	0.612

Table 4 Estimated $\widehat{\mathrm{VRF}}$ and $\hat{\nu}$ for the criteria $\mathcal{P}_{\gamma,2}$ and $\mathcal{M}'_{\gamma,2}$, and for selected types of weights, for the basic estimator with $x = 60$ (top) and 85 (bottom) without the baker's transformation. Projection-dependent, order-dependent and geometric order-dependent are respectively abbreviated by *proj.-dep.*, *order-dep.*, *geometric*. The results are sorted by decreasing order of $\hat{\nu}$.

weight type	without baker			with baker		
	$\widehat{\mathrm{VRF}}(2^{20})$	$\hat{\nu}$	$\hat{S}_\varepsilon$	$\widehat{\mathrm{VRF}}(2^{20})$	$\hat{\nu}$	$\hat{S}_\varepsilon$
proj.-dep.	8.0×10^2	1.469 ± 0.004	0.265	8.2×10^2	1.380 ± 0.010	0.666
product	8.7×10^2	1.499 ± 0.005	0.338	1.3×10^3	1.422 ± 0.007	0.512
order-dep.	5.6×10^2	1.486 ± 0.005	0.339	7.5×10^2	1.402 ± 0.009	0.602
geometric	4.9×10^2	1.460 ± 0.006	0.462	8.4×10^2	1.413 ± 0.008	0.585

Table 5 Estimated $\widehat{\mathrm{VRF}}$, $\hat{\nu}$ and $\hat{S}_\varepsilon$ for the RQMC estimator of $\mathbb{E}[T]$ for the criterion $\mathcal{P}_{\gamma,2\alpha}$ with $\alpha = 1$ and 2 without and with the baker's transformation, respectively.

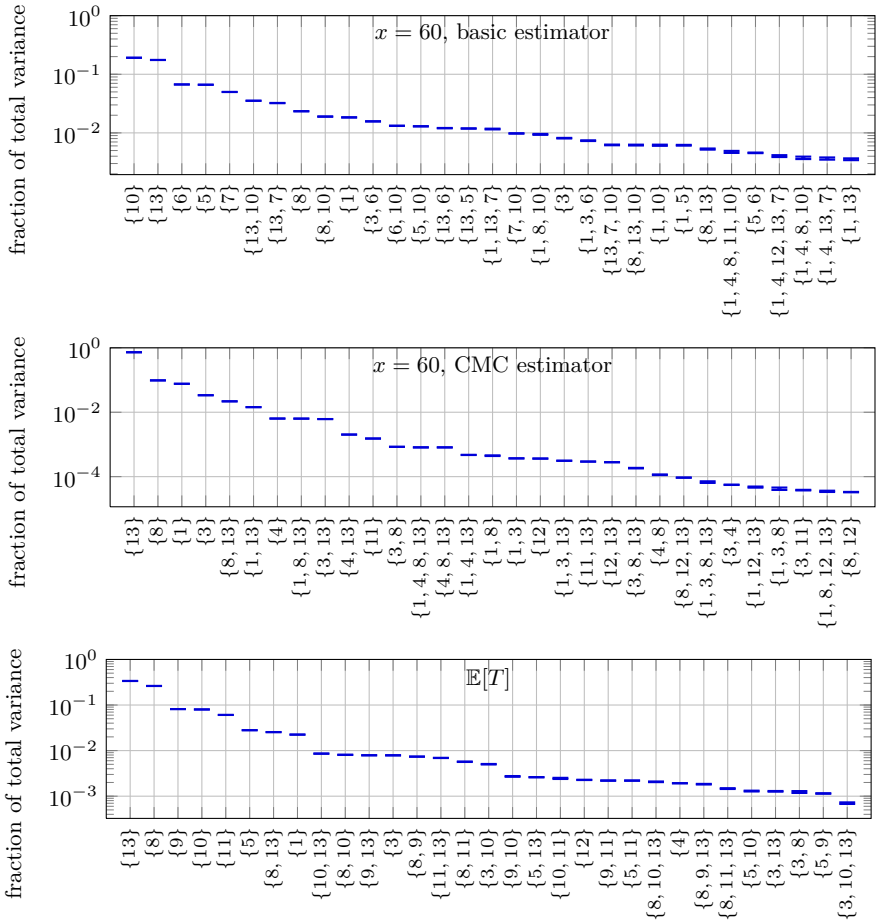

Fig. 12 Fractional ANOVA variances per projection for the stochastic activity network example with $x = 60$ for the basic estimator (top), the CMC estimator (middle), and the estimator of $\mathbb{E}[T]$ (bottom). Note the different vertical scales. Only the 31 more important projections out of $2^{13} - 1 = 8191$ (basic estimator) or $2^8 - 1 = 255$ (CMC estimator) total projections are displayed. See Figure 9 for details on how to read this figure.

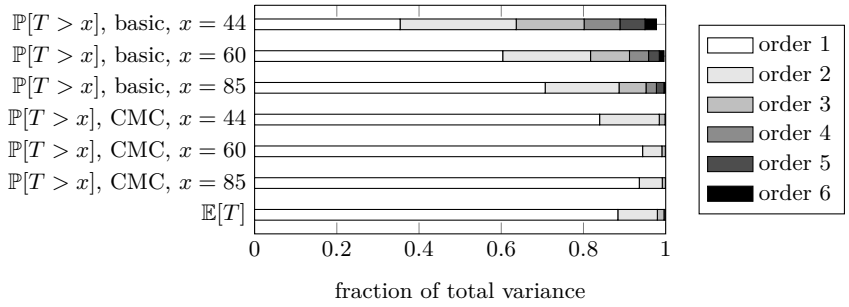

Fig. 13 Fractional ANOVA variances per projection order, up to order 6, for the stochastic activity network example.

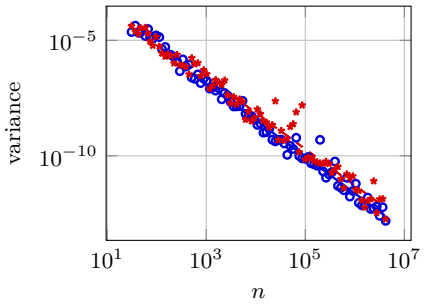

Fig. 14 Estimated variance of the RQMC estimator using the baker's transformation for the stochastic activity network with $x = 44$, for the $\mathcal{P}_{\gamma,4}$ criterion (○) and for the $\mathcal{M}'_{\gamma,2}$ criterion (⋆), both with projection-dependent weights. The results for $\mathcal{M}_{\gamma,2}$ (not shown here) are similar to those for $\mathcal{M}'_{\gamma,2}$.

15 Example: Asian Call Option

Most of the results for the Asian call option were already presented in Section 11. We show in Figures 15 and 16 the estimated ANOVA variances for the most important projections, and in Figure 17 the total variance per projection order.

We show in Table 6 the fitted VRF's and empirical convergence rates for various types of weights with the $\mathcal{P}_{\gamma,2\alpha}$ criterion using random CBC construction, and for projection-dependent weights for the $\mathcal{M}_{\gamma,2}$ and $\mathcal{M}'_{\gamma,2}$ criteria, but for the Cholesky case instead of PCA like in Table 1 in the main paper. Also for Cholesky, we show in Table 7 the fitted VRF's and the constants $\ln \hat{a}_0$ and $\hat{\nu}$ for criteria $\mathcal{M}_{\gamma,\beta}$, $\mathcal{M}'_{\gamma,\beta}$, $\widetilde{\mathcal{M}}_{\gamma,\beta}$ and $\widetilde{\mathcal{M}}'_{\gamma,\beta}$, for $\beta = 1$ and 2, and for projection-dependent, product, order-dependent and geometric order-dependent weights. In general, $\ln \hat{a}_0$ decreases as $\hat{\nu}$ increases, as illustrated in Figure 4, and the criteria $\widetilde{\mathcal{M}}_{\gamma,\beta}$ and $\widetilde{\mathcal{M}}'_{\gamma,\beta}$, based on the worst projection, generally yield faster convergence and larger VRF than their counterparts $\mathcal{M}_{\gamma,\beta}$ and $\mathcal{M}'_{\gamma,\beta}$ based on a weighted sum over all projections. Besides this, it is hard to discriminate between criteria and weight types. For example, for

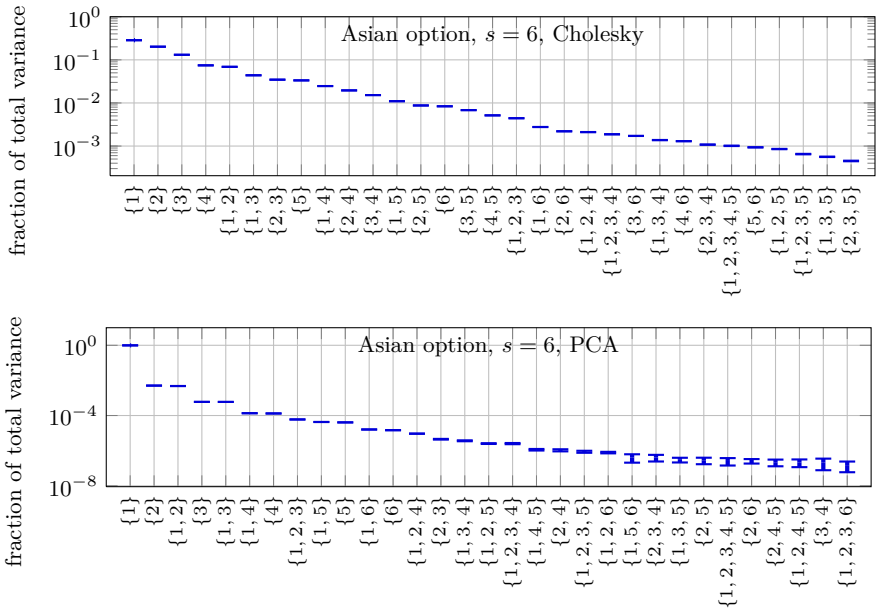

Fig. 15 Fractional ANOVA variances per projection for the Asian option with $s = 6$ using Cholesky factorization (top) and PCA decomposition (bottom). Only the 31 most important projections out of $2^6 - 1 = 63$ total projections are displayed. The two plots here have different vertical scales and the contributions decrease much faster in the bottom one.

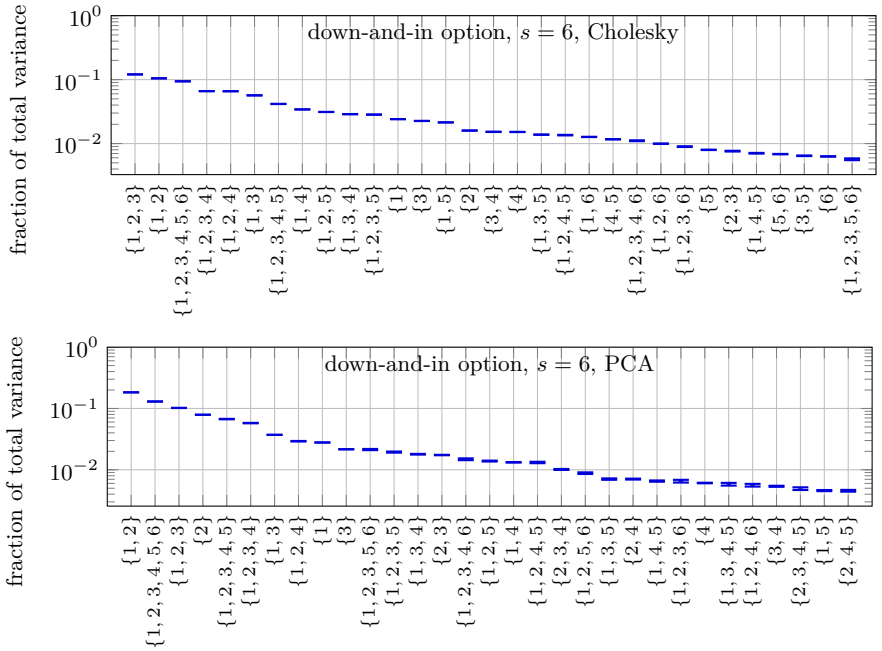

Fig. 16 Fractional ANOVA variances per projection for the down-and-in Asian option with $s = 6$ using Cholesky factorization (top) and PCA decomposition (bottom). Only the 31 most important projections out of $2^6 - 1 = 63$ total projections are displayed.

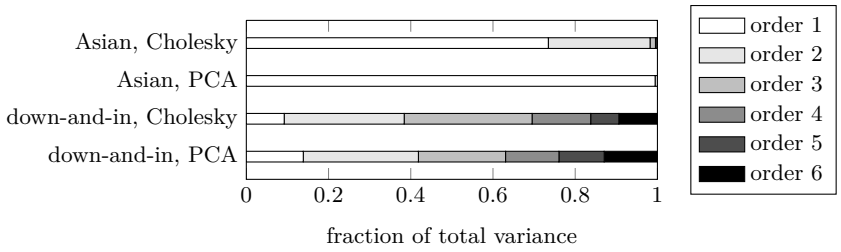

Fig. 17 Fractional ANOVA variance per projection order for the Asian option and the down-and-in Asian option with $s = 6$.

$\widetilde{\mathcal{M}}'_{\gamma,1}$, product and projection-dependent weights yield $\hat{\nu} \approx 1.74$ and 1.42, respectively, whereas for $\widetilde{\mathcal{M}}_{\gamma,1}$, they yield $\hat{\nu} \approx 1.45$ and 1.69, respectively, which is nearly the converse.

Asian option (Cholesky), $s = 6$

criterion	construction	r	weight type	$\widehat{\mathrm{VRF}}(2^{20})$	$\hat{\nu}$	$\hat{S}_\varepsilon$
$\mathcal{P}_{\gamma,4}$	CBC	50	proj.-dep.	4.2×10^3	1.425 ± 0.006	0.454
			product	3.1×10^3	1.384 ± 0.008	0.590
			order-dep.	4.1×10^3	1.454 ± 0.006	0.483
			geometric	4.5×10^3	1.470 ± 0.005	0.408
			order 2	1.3×10^3	1.430 ± 0.020	1.47
		–	proj.-dep.	5×10^3	1.460 ± 0.010	0.272
	Korobov	50	proj.-dep.	2.7×10^3	1.410 ± 0.007	0.511
		–	proj.-dep.	5.1×10^3	1.510 ± 0.020	0.379
$\mathcal{M}_{\gamma,2}$	CBC	50	proj.-dep.	1.4×10^3	1.380 ± 0.010	1.08
$\mathcal{M}'_{\gamma,2}$	CBC	50	proj.-dep.	1.7×10^3	1.335 ± 0.009	0.705

down-and-in option (Cholesky), $s = 6$

criterion	construction	r	weight type	$\widehat{\mathrm{VRF}}(2^{20})$	$\hat{\nu}$	$\hat{S}_\varepsilon$
$\mathcal{P}_{\gamma,4}$	CBC	50	proj.-dep.	9.3	1.224 ± 0.004	0.321
			product	10	1.262 ± 0.004	0.319
			order-dep.	9.9	1.250 ± 0.004	0.268
			geometric	9.4	1.251 ± 0.005	0.398
			order 2	4.2	1.210 ± 0.010	0.804
		–	proj.-dep.	12	1.267 ± 0.007	0.179
	Korobov	50	proj.-dep.	8.2	1.242 ± 0.004	0.267
		–	proj.-dep.	11	1.286 ± 0.007	0.192
$\mathcal{M}_{\gamma,2}$	CBC	50	proj.-dep.	6.7	1.229 ± 0.006	0.475
$\mathcal{M}'_{\gamma,2}$	CBC	50	proj.-dep.	6.0	1.198 ± 0.008	0.560

Table 6 Fitted variance reduction factors at $n = 2^{20}$ and empirical convergence rates for the Asian and down-and-in options. The baker's transformation was applied for the Asian option, but not for the down-and-in option. When CBC is followed by a value of r, it refers to random CBC, otherwise it refers to exhaustive CBC, and similarly for Korobov. Order-dependent of order 2 is abbreviated as *order 2*.

criterion	weight type	$\widehat{\mathrm{VRF}}(2^{20})$	$\ln \hat{a}_0$	$\hat{\nu}$	$\hat{S}_\varepsilon$
$\widetilde{\mathcal{M}}'_{\gamma,1}$	product	3.2×10^3	8.6 ± 0.1	1.74 ± 0.01	0.918
$\widetilde{\mathcal{M}}'_{\gamma,1}$	order-dep.	3.0×10^3	8.5 ± 0.1	1.73 ± 0.01	0.887
$\widetilde{\mathcal{M}}_{\gamma,1}$	proj.-dep.	2.5×10^3	8.2 ± 0.2	1.69 ± 0.01	1.00
$\widetilde{\mathcal{M}}_{\gamma,2}$	proj.-dep.	2.5×10^3	8.2 ± 0.2	1.69 ± 0.01	1.00
$\widetilde{\mathcal{M}}'_{\gamma,2}$	product	2.7×10^3	7.9 ± 0.1	1.68 ± 0.01	0.780
$\widetilde{\mathcal{M}}'_{\gamma,2}$	order-dep.	2.1×10^3	7.8 ± 0.1	1.65 ± 0.01	0.964
$\widetilde{\mathcal{M}}'_{\gamma,1}$	geometric	2.0×10^3	7.5 ± 0.1	1.63 ± 0.01	0.933
$\widetilde{\mathcal{M}}_{\gamma,1}$	order-dep.	2.4×10^3	5.9 ± 0.2	1.53 ± 0.01	1.10
$\widetilde{\mathcal{M}}_{\gamma,1}$	geometric	2.6×10^3	5.5 ± 0.1	1.50 ± 0.01	0.843
$\mathcal{M}_{\gamma,2}$	product	1.9×10^3	5.4 ± 0.2	1.47 ± 0.01	0.989
$\mathcal{M}_{\gamma,1}$	order-dep.	1.7×10^3	5.4 ± 0.1	1.47 ± 0.01	0.956
$\widetilde{\mathcal{M}}_{\gamma,2}$	product	2.0×10^3	5.2 ± 0.1	1.46 ± 0.01	0.941
$\widetilde{\mathcal{M}}_{\gamma,2}$	order-dep.	2.1×10^3	5.1 ± 0.1	1.46 ± 0.01	0.932
$\widetilde{\mathcal{M}}_{\gamma,1}$	product	1.8×10^3	5.2 ± 0.2	1.45 ± 0.01	1.09
$\mathcal{M}_{\gamma,2}$	order-dep.	1.5×10^3	5.3 ± 0.2	1.45 ± 0.01	1.04
$\widetilde{\mathcal{M}}_{\gamma,2}$	geometric	2.8×10^3	4.7 ± 0.1	1.45 ± 0.01	0.562
$\mathcal{M}'_{\gamma,2}$	geometric	2.5×10^3	4.5 ± 0.1	1.43 ± 0.01	0.650
$\widetilde{\mathcal{M}}'_{\gamma,1}$	proj.-dep.	1.2×10^3	5.2 ± 0.2	1.42 ± 0.02	1.53
$\mathcal{M}_{\gamma,1}$	product	1.6×10^3	4.9 ± 0.1	1.42 ± 0.01	0.973
$\mathcal{M}'_{\gamma,1}$	order-dep.	1.9×10^3	4.6 ± 0.1	1.42 ± 0.01	0.887
$\mathcal{M}_{\gamma,2}$	geometric	2.0×10^3	4.6 ± 0.1	1.42 ± 0.01	0.763
$\mathcal{M}_{\gamma,1}$	proj.-dep.	1.6×10^3	4.7 ± 0.1	1.41 ± 0.01	0.870
$\mathcal{M}'_{\gamma,1}$	geometric	1.8×10^3	4.5 ± 0.1	1.41 ± 0.01	0.723
$\widetilde{\mathcal{M}}'_{\gamma,2}$	proj.-dep.	1.8×10^3	4.4 ± 0.1	1.40 ± 0.01	0.670
$\mathcal{M}'_{\gamma,2}$	order-dep.	1.9×10^3	4.3 ± 0.1	1.40 ± 0.01	0.635
$\mathcal{M}_{\gamma,1}$	geometric	2.0×10^3	4.2 ± 0.1	1.39 ± 0.01	0.673
$\mathcal{M}_{\gamma,2}$	proj.-dep.	1.4×10^3	4.4 ± 0.2	1.38 ± 0.01	1.08
$\mathcal{M}'_{\gamma,1}$	proj.-dep.	1.9×10^3	4.0 ± 0.1	1.38 ± 0.01	0.690
$\mathcal{M}'_{\gamma,2}$	product	1.6×10^3	4.2 ± 0.1	1.37 ± 0.01	0.860
$\mathcal{M}'_{\gamma,1}$	product	1.4×10^3	4.1 ± 0.1	1.36 ± 0.01	0.972
$\mathcal{M}'_{\gamma,2}$	proj.-dep.	1.7×10^3	3.6 ± 0.1	1.34 ± 0.01	0.705
$\widetilde{\mathcal{M}}'_{\gamma,2}$	geometric	1.0×10^3	3.6 ± 0.2	1.30 ± 0.02	1.12
$\mathcal{P}_{\gamma,4}$	geometric	4.5×10^3	4.50 ± 0.06	1.470 ± 0.005	0.408
$\mathcal{P}_{\gamma,4}$	order-dep.	4.1×10^3	4.36 ± 0.07	1.454 ± 0.006	0.483
$\mathcal{P}_{\gamma,4}$	order 2	1.3×10^3	5.20 ± 0.20	1.430 ± 0.020	1.47
$\mathcal{P}_{\gamma,4}$	proj.-dep.	4.2×10^3	3.93 ± 0.07	1.425 ± 0.006	0.454
$\mathcal{P}_{\gamma,4}$	product	3.1×10^3	3.70 ± 0.10	1.384 ± 0.008	0.590

Table 7 Estimated $\widehat{\mathrm{VRF}}$, $\hat{\nu}$ and $\hat{S}_\varepsilon$ for the criteria based on the spectral test $\mathcal{M}_{\gamma,\beta}$, $\mathcal{M}'_{\gamma,\beta}$, $\widetilde{\mathcal{M}}_{\gamma,\beta}$ and $\widetilde{\mathcal{M}}'_{\gamma,\beta}$, for $\beta = 1$ and 2, and for projection-dependent, product, order-dependent and geometric order-dependent weights, for the Asian option with Cholesky factorization with the baker's transformation. The results are sorted by decreasing order of $\hat{\nu}$. We have appended the results for $\mathcal{P}_{\gamma,4}$ for reference.